Research Square

Preprints are preliminary reports that have not undergone peer review.
They should not be considered conclusive, used to inform clinical practice,
or referenced by the media as validated information.

Numerical Solution of Coupled Emden-FowlerEquations Using Haar Wavelet Collocation Method

Arushi .
Sri Venkateswara College
Pranay Goswami
pranay@aud.ac.in
Ambedkar University Delhi
Saad Althobaiti
Taif University

Research Article

Keywords: Coupled system of Emden-Fowler equations, Numerical method, Haar wavelet collocation method, Deep neural network techniques.

Posted Date: March 11th, 2026

DOI: https://doi.org/10.21203/rs.3.rs-8936364/v1

License: This work is licensed under a Creative Commons Attribution 4.0 International License.
Read Full License

Additional Declarations: No competing interests reported.

Numerical Solution of Coupled Emden-Fowler Equations Using Haar Wavelet Collocation Method

Arushi
Sri Venkateswara College, University of Delhi, Delhi 110021, India;
E-mails: arushi.garvita@gmail.com, arushi@svc.ac.in
Pranay Goswami*
Dr. B. R. Ambedkar University Delhi, Delhi 110006, India;
E-mail: pranay@aud.ac.in, pranaygoswami83@gmail.com
Saad Althobaiti
Department of Science and Technology, University College Ranyah,
Taif University, Ranyah, 21975, Saudi Arabia;
E-mail: snthobaiti@tu.edu.sa

February 19, 2026

Abstract

This paper presents a numerical scheme for solving coupled systems of Emden-Fowler equations based on the Haar wavelet collocation method (HWCM). This method converts the system of singular differential equations into a set of algebraic equations by approximating the higher-order derivatives using wavelet techniques. Newton's method is used to solve the resulting nonlinear system and obtain the Haar coefficients. Numerical experiments on several benchmark problems demonstrate the precision and effectiveness of the proposed approach. The results show excellent agreement with exact solutions and compare favorably with existing methods, including artificial neural network (ANN) techniques. The method is extended to coupled systems for the first time, achieving errors of order 10^{-3} to 10^{-6} with a theoretical convergence rate of $O(2^{-3L/2})$. The method is implemented in Mathematica, and comprehensive error tables and graphical comparisons are provided. HWCM is shown to be a robust, deterministic alternative to data-driven methods for solving coupled singular differential systems in astrophysics and related fields.

Keywords: Coupled system of Emden-Fowler equations, Numerical method, Haar wavelet collocation method, Deep neural network techniques.

MSC: Primary 34A34, 34K37, 34K28, 65L60, 65T60.

**Corresponding author

1 Introduction

Differential equations play an important role in the mathematical modelling. Many phenomena governed by conservation laws, force balances, or transport mechanisms are naturally expressed through ordinary or partial differential equations. Among these, singular boundary and initial value problems present particular analytical and numerical challenges due to the presence of non-regular coefficients or undefined terms at specific points in the domain (see [1, 2]). Among differential equations, the class of singular boundary value problems known as Emden-Fowler equations holds particular historical and practical significance, especially in the field of astrophysics. These equations arise in the study of stellar structure and hydrostatic equilibrium in self-gravitating gaseous spheres [3].

The Lane-Emden equation was produced to report the internal construction of polytropic stars under the premise of hydrostatic equilibrium in 1870 [4]. This was later generalised in [5], which demostrated the mathematical structure for examining the distribution of temperature in stellar bodies. Let n be the polytropic index governing the equation of state, then the classical Lane-Emden equation is expressed as:

$$\frac{d^2\omega}{d\zeta^2} + \frac{2}{\zeta}\frac{d\omega}{d\zeta} + \omega^n = 0, \tag{1}$$

This work was further expanded in [6, 7] during 1914-1931 by including more complex nonlinearities and source terms which resulted in a new class of Endem-Fowler equation:

$$\frac{d^2\omega}{d\zeta^2} + \frac{\vartheta}{\zeta}\frac{d\omega}{d\zeta} + \varphi(\omega) = \psi(\zeta), \tag{2}$$

where $\varphi(\omega)$ denotes a linear or nonlinear function of the dependent variable and $\psi(\zeta)$ represents an external forcing function. The singular coefficient $\frac{\vartheta}{\zeta}$ is challenging as the standard numerical methods fail due to $\zeta = 0$.

Coupled systems of Emdem-Fowler equations arise in numerous applications, including multi-component stellar models in astrophysics, reaction-diffusion processes in chemical engineering, and thermoelasticity. The general form of such coupled systems can be expressed as:

$$\begin{aligned} \frac{d^2\omega_1}{d\zeta^2} + \frac{\vartheta_1}{\zeta}\frac{d\omega_1}{d\zeta} &= \varphi_1(\zeta, \omega_1, \omega_2), \\ \frac{d^2\omega_2}{d\zeta^2} + \frac{\vartheta_2}{\zeta}\frac{d\omega_2}{d\zeta} &= \varphi_2(\zeta, \omega_1, \omega_2), \end{aligned} \tag{3}$$

where $\vartheta_1, \vartheta_2 > 0$ are real constants, and φ_1, φ_2 are nonlinear functions representing the coupling between the components.

Emden-Fowler equations are difficult to solve due to non linearity and $\zeta = 0$. To deal with this many analytical and numerical methods have been developed like power series expansions and perturbation procedures [22]. Semi-analytical techniques, including the variational iteration method (VIM) [10], homotopy perturbation method (HPM) [9], homotopy analysis method (HAM) [8], and Adomian decomposition method (ADM) [11] have been effectively used in more recent times. Finite difference methods, spectral methods, and collocation techniques employing different basis functions, such as Bernstein

polynomials, have all been used in numerical dealings [12].

One of the many advancements in the recent years includes the application of artificial intelligence methods to solve such systems. Singular boundary value problems being one of the types of differential equations for which Artificial Neural Networks (ANNs) have become effective tools for solving [13]. They have the advantage of being able to solve complex nonlinearities without explicitly discretizing the differential operators. However, they also have drawbacks, including the need for large amounts of training data, hyper-parameter tuning, and issues with interpretability and convergence guarantees.

Additionally, numerical techniques based on wavelet theory are of importance due to their superior approximation qualities and multiresolution capabilities. Because of their computing efficiency, orthogonality, compact support, and mathematical simplicity, Haar wavelets have been of special interest for numerical computations among different wavelet families [14, 15]. Numerous classes of differential equations, such as fractional differential equations [18], higher-order boundary value problems [16], and single Emden-Fowler equations [17], have been effectively solved using the HWCM. This approach uses a Haar wavelet series to estimate the highest-order derivative, which is then integrated to get approximations for lower-order derivatives and the solution. This method converts the differential problem into a system of algebraic equations that Newton's method and other common nonlinear solvers can solve. Recently there have been research on the study of Zika virus transmission, Hepatitis B Virus, Diabetes and effects of global warming on marine ecosystems using Haar wavelet method [24], [25], [26], [27], [28].

Although HWCM has been successfully applied to single Emdem-Fowler equations, its extension to coupled systems has received little attention in the literature. The coupled systems are more reflective of real-world physical events than their single-equation equivalents,therefore, there is a need of research in this area. Furthermore, a thorough comparison with deterministic wavelet approaches is absent, despite recent work showing the efficacy of ANN methods for coupled Emden-Fowler systems [13]. Understanding the relative advantages and disadvantages of data-driven vs conventional numerical techniques for singular differential systems requires such a comparison.

By providing the first thorough application of the Haar wavelet collocation approach to coupled systems of Emden-Fowler equations, this work seeks to close this significant gap. Our work significantly advances the field in a number of ways:

1. We create a comprehensive HWCM framework designed especially for connected single systems.

2. We offer convergence analysis for coupled systems using HWCM.

3. We apply the method in Mathematica and evaluate it on five benchmark coupled systems selected from current research [19, 21].

4. We provide a thorough comparison with ANN techniques [13], highlighting the competitive advantages of HWCM in terms of numerical accuracy, computational effectiveness, and ease of implementation.

The paper is organized as follows: Section 2 presents mathematical preliminaries of Haar wavelets. Section 3 describes the HWCM methodology for coupled systems. Section 4

presents a convergence analysis. Section 5 presents detailed numerical experiments on five benchmark problems. Section 6 discusses results of numerical analysis based on Mathematica and earlier sections. Section 7 compares HWCM with ANN method. Section 8 concludes with implications.

2 Haar Wavelet Preliminaries

Haar wavelets consist of piecewise constant functions that take values 1, -1, and 0. For the interval $[0, 1]$, with resolution level L, let $K = 2^L$ denote the number of subintervals. The total number of wavelet functions is $2K$.

2.1 Definition of Haar Wavelet Family

The scaling function (corresponding to $j = 1$) is defined as:

$$h_1(\zeta) = 1, \quad \zeta \in [0, 1]. \tag{4}$$

For $j \geq 2$, the Haar wavelet functions are defined as:

$$h_j(\zeta) = \begin{cases} 1, & \xi_1 \leq \zeta < \xi_2, \\ -1, & \xi_2 \leq \zeta < \xi_3, \\ 0, & \text{otherwise}, \end{cases} \tag{5}$$

where the parameters ξ_1, ξ_2, ξ_3 are determined by the dilation parameter l and translation parameter λ as follows:

$$\xi_1 = \frac{\lambda}{2^l}, \quad \xi_2 = \frac{\lambda + \frac{1}{2}}{2^l}, \quad \xi_3 = \frac{\lambda + 1}{2^l}. \tag{6}$$

The index j is related to l and λ by:

$$j = 2^l + \lambda + 1, \quad l = 0, 1, \ldots, L, \quad \lambda = 0, 1, \ldots, 2^l - 1. \tag{7}$$

Thus, as l increases from 0 to L, the wavelets provide a multiresolution analysis of the interval $[0, 1]$, with each level l containing 2^l wavelets of support width 2^{-l}.

2.2 Multiple Integrals of Haar Wavelets

For numerical solution of differential equations, we require repeated integrals of Haar wavelets. Define the p-fold integral recursively as:

$$\rho_{j,1}(\zeta) = \int_0^\zeta h_j(t)\, dt, \tag{8}$$

$$\rho_{j,p}(\zeta) = \int_0^\zeta \rho_{j,p-1}(t)\, dt, \quad p \geq 2. \tag{9}$$

For the scaling function $j = 1$, these integrals have the simple form:

$$\rho_{1,p}(\zeta) = \frac{\zeta^p}{p!}, \quad p \geq 1. \tag{10}$$

For $j \geq 2$ with support $[\xi_1, \xi_2, \xi_3]$, the first integral is given by the piecewise linear function:

$$\rho_{j,1}(\zeta) = \begin{cases} 0, & 0 \leq \zeta < \xi_1, \\ \zeta - \xi_1, & \xi_1 \leq \zeta < \xi_2, \\ \xi_3 - \zeta, & \xi_2 \leq \zeta < \xi_3, \\ 0, & \xi_3 \leq \zeta \leq 1. \end{cases} \tag{11}$$

The second integral, obtained by integrating $\rho_{j,1}$, gives:

$$\rho_{j,2}(\zeta) = \begin{cases} 0, & 0 \leq \zeta < \xi_1, \\ \dfrac{1}{2}(\zeta - \xi_1)^2, & \xi_1 \leq \zeta < \xi_2, \\ \dfrac{1}{2}\left(\dfrac{1}{2^l}\right)^2 - \dfrac{1}{2}(\xi_3 - \zeta)^2, & \xi_2 \leq \zeta < \xi_3, \\ \dfrac{1}{2}\left(\dfrac{1}{2^l}\right)^2, & \xi_3 \leq \zeta \leq 1. \end{cases} \tag{12}$$

Observe that $\xi_3 - \xi_1 = 1/2^l$. This is the reason for the constant term in the third and fourth branches. For higher-order integrals ($p \geq 3$), one can continue the recursive process. For second-order differential equations only $\rho_{j,1}$ and $\rho_{j,2}$ are required.

2.3 Function Approximation

Any function $f \in L^2[0,1]$ can be expanded in the Haar wavelet series:

$$f(\zeta) = \sum_{j=1}^{\infty} \alpha_j h_j(\zeta), \tag{13}$$

where the coefficients are given by the inner product $\alpha_j = \langle f, h_j \rangle = \int_0^1 f(\zeta) h_j(\zeta)\, d\zeta$. The series converges in the L^2 norm. For continuous functions with bounded variation, the convergence is uniform except at points of discontinuity.
For numerical computation, we truncate the series at resolution level L, retaining $2K$ terms where $K = 2^L$:

$$f(\zeta) \approx \sum_{j=1}^{2K} \hat{\alpha}_j h_j(\zeta). \tag{14}$$

The accuracy of this approximation improves as L increases, with the error decaying as $O(2^{-3L/2})$ for sufficiently smooth functions [18].

3 Haar Wavelet Collocation Method for Coupled Systems

3.1 Problem Formulation

We consider coupled systems of second-order Emden-Fowler equations on the interval $(0, 1]$ with initial conditions at the singular point $\zeta = 0$:

$$\begin{cases} \dfrac{d^2\omega_1}{d\zeta^2} + \dfrac{\theta_1}{\zeta}\dfrac{d\omega_1}{d\zeta} = \phi_1(\zeta, \omega_1, \omega_2), \\ \dfrac{d^2\omega_2}{d\zeta^2} + \dfrac{\theta_2}{\zeta}\dfrac{d\omega_2}{d\zeta} = \phi_2(\zeta, \omega_1, \omega_2), \end{cases} \qquad \zeta \in (0, 1], \tag{15}$$

subject to the initial conditions:

$$\omega_1(0) = a_1, \quad \omega_1'(0) = b_1, \quad \omega_2(0) = a_2, \quad \omega_2'(0) = b_2. \tag{16}$$

Here $\theta_1, \theta_2 > 0$ are constants, and ϕ_1, ϕ_2 are sufficiently smooth nonlinear functions representing the coupling between the components.

4 Haar Wavelet Collocation Method for Coupled Systems

4.1 Problem Formulation

We consider coupled systems of second-order Emden-Fowler equations on the interval $(0, 1]$ with initial conditions at the singular point $\zeta = 0$:

$$\begin{cases} \dfrac{d^2\omega_1}{d\zeta^2} + \dfrac{\theta_1}{\zeta}\dfrac{d\omega_1}{d\zeta} = \phi_1(\zeta, \omega_1, \omega_2), \\ \dfrac{d^2\omega_2}{d\zeta^2} + \dfrac{\theta_2}{\zeta}\dfrac{d\omega_2}{d\zeta} = \phi_2(\zeta, \omega_1, \omega_2), \end{cases} \qquad \zeta \in (0, 1], \tag{17}$$

subject to the initial conditions:

$$\omega_1(0) = a_1, \quad \omega_1'(0) = b_1, \quad \omega_2(0) = a_2, \quad \omega_2'(0) = b_2. \tag{18}$$

Here $\theta_1, \theta_2 > 0$ are constants, and ϕ_1, ϕ_2 are sufficiently smooth nonlinear functions representing the coupling between the components.

4.2 Haar Wavelet Approximation

The fundamental principle of the Haar wavelet collocation method is to expand the highest-order derivatives in the Haar series. For our second-order system, we set:

$$\frac{d^2\omega_1}{d\zeta^2} = \sum_{j=1}^{2K} \alpha_j h_j(\zeta), \quad \frac{d^2\omega_2}{d\zeta^2} = \sum_{j=1}^{2K} \beta_j h_j(\zeta), \tag{19}$$

where $\boldsymbol{\alpha} = (\alpha_1, \alpha_2, \ldots, \alpha_{2K})^T$ and $\boldsymbol{\beta} = (\beta_1, \beta_2, \ldots, \beta_{2K})^T$ are vectors of unknown Haar coefficients to be determined.

4.3 Integration and Incorporation of Initial Conditions

Integrating (19) from 0 to ζ and applying the initial conditions for first derivatives gives:

$$\frac{d\omega_1}{d\zeta} = \sum_{j=1}^{2K} \alpha_j \rho_{j,1}(\zeta) + b_1, \quad \frac{d\omega_2}{d\zeta} = \sum_{j=1}^{2K} \beta_j \rho_{j,1}(\zeta) + b_2, \tag{20}$$

where $\rho_{j,1}(\zeta) = \int_0^\zeta h_j(t)\, dt$.

Integrating again and applying the initial conditions gives:

$$\begin{aligned} \omega_1(\zeta) &= \sum_{j=1}^{2K} \alpha_j \rho_{j,2}(\zeta) + \zeta b_1 + a_1, \\ \omega_2(\zeta) &= \sum_{j=1}^{2K} \beta_j \rho_{j,2}(\zeta) + \zeta b_2 + a_2, \end{aligned} \tag{21}$$

where $\rho_{j,2}(\zeta) = \int_0^\zeta \rho_{j,1}(t)\, dt$.

4.4 Collocation Points and Residual Formation

Let the collocation points be defined as:

$$\zeta_i = \frac{i - 0.5}{2K}, \quad i = 1, 2, \ldots, 2K. \tag{22}$$

These collocation points are evenly distributed and avoid the singular point $\zeta = 0$. As the resolution increases, the first collocation point $\zeta_1 = 1/(4K)$ approaches zero, thus avoiding evaluation at the singularity.

4.5 Residual Equations

Substituting (21) and (20) into (17) at the collocation points yields a system of $4K$ nonlinear algebraic equations. For $i = 1, 2, \ldots, 2K$:

$$\begin{aligned} F_1^i(\boldsymbol{\alpha}, \boldsymbol{\beta}) = &\sum_{j=1}^{2K} \alpha_j h_j(\zeta_i) + \frac{\theta_1}{\zeta_i} \left(\sum_{j=1}^{2K} \alpha_j \rho_{j,1}(\zeta_i) + b_1 \right) \\ &- \phi_1 \left(\zeta_i, \sum_{j=1}^{2K} \alpha_j \rho_{j,2}(\zeta_i) + \zeta_i b_1 + a_1, \sum_{j=1}^{2K} \beta_j \rho_{j,2}(\zeta_i) + \zeta_i b_2 + a_2 \right) = 0, \end{aligned} \tag{23}$$

$$\begin{aligned} F_2^i(\boldsymbol{\alpha}, \boldsymbol{\beta}) = &\sum_{j=1}^{2K} \beta_j h_j(\zeta_i) + \frac{\theta_2}{\zeta_i} \left(\sum_{j=1}^{2K} \beta_j \rho_{j,1}(\zeta_i) + b_2 \right) \\ &- \phi_2 \left(\zeta_i, \sum_{j=1}^{2K} \alpha_j \rho_{j,2}(\zeta_i) + \zeta_i b_1 + a_1, \sum_{j=1}^{2K} \beta_j \rho_{j,2}(\zeta_i) + \zeta_i b_2 + a_2 \right) = 0. \end{aligned} \tag{24}$$

4.6 The Nonlinear System

Define the combined unknown vector $\mathbf{X} \in \mathbb{R}^{4K}$ as:

$$\mathbf{X} = [\alpha_1, \alpha_2, \ldots, \alpha_{2K}, \beta_1, \beta_2, \ldots, \beta_{2K}]^T, \tag{25}$$

and the residual vector $\mathbf{F}(\mathbf{X}) \in \mathbb{R}^{4K}$ as:

$$\mathbf{F}(\mathbf{X}) = [F_1^1, F_1^2, \ldots, F_1^{2K}, F_2^1, F_2^2, \ldots, F_2^{2K}]^T. \tag{26}$$

We have now transformed the coupled differential system into a nonlinear algebraic system:

$$\mathbf{F}(\mathbf{X}) = \mathbf{0}. \tag{27}$$

4.7 Newton's Method for the Nonlinear System

We solve $\mathbf{F}(\mathbf{X}) = \mathbf{0}$ using Newton's iteration. At each step k, we solve the linear system:

$$\mathbf{J}(\mathbf{X}^{(k)})\Delta\mathbf{X}^{(k)} = -\mathbf{F}(\mathbf{X}^{(k)}), \tag{28}$$

and update:

$$\mathbf{X}^{(k+1)} = \mathbf{X}^{(k)} + \Delta\mathbf{X}^{(k)}, \tag{29}$$

where $\mathbf{J}(\mathbf{X}) \in \mathbb{R}^{4K\times 4K}$ is the Jacobian matrix with entries $J_{pq} = \partial F_p/\partial X_q$.

4.7.1 Jacobian Structure

The Jacobian exhibits a natural block structure reflecting the coupling between equations:

$$\mathbf{J} = \begin{pmatrix} \dfrac{\partial \mathbf{F}_1}{\partial \boldsymbol{\alpha}} & \dfrac{\partial \mathbf{F}_1}{\partial \boldsymbol{\beta}} \\ \dfrac{\partial \mathbf{F}_2}{\partial \boldsymbol{\alpha}} & \dfrac{\partial \mathbf{F}_2}{\partial \boldsymbol{\beta}} \end{pmatrix}, \tag{30}$$

where each block is a $2K \times 2K$ matrix.

4.8 Initialization and Convergence Criteria

The convergence of Newton's method depends critically on the initial guess $\mathbf{X}^{(0)}$. We employ the zero-coefficient initialization strategy, setting $\alpha_j = \beta_j = 0$ for all j, which corresponds to approximating the solutions by the linear terms from initial conditions:

$$\omega_1(\zeta) \approx a_1 + \zeta b_1, \quad \omega_2(\zeta) \approx a_2 + \zeta b_2. \tag{31}$$

The Newton iteration is terminated when either of the following criteria is satisfied:

$$\|\mathbf{F}(\mathbf{X}^{(k)})\|_\infty < \epsilon_{\text{abs}} \quad \text{or} \quad \|\Delta\mathbf{X}^{(k)}\|_\infty < \epsilon_{\text{rel}}\|\mathbf{X}^{(k)}\|_\infty, \tag{32}$$

with typical tolerances $\epsilon_{\text{abs}} = 10^{-12}$ and $\epsilon_{\text{rel}} = 10^{-10}$. A maximum of $k_{\max} = 50$ iterations is imposed to prevent infinite loops in case of non-convergence.

4.9 Treatment of the Singular Point

A key advantage of the proposed method is its natural handling of the singularity at $\zeta = 0$. The collocation points (22) are chosen to avoid $\zeta = 0$, with the nearest point at distance $1/(4K)$. To prevent numerical division by zero in the implementation, we apply a small cutoff:

$$\text{If } \zeta_i < 10^{-10}, \text{ set } \zeta_i = 10^{-10}. \tag{33}$$

The initial conditions at the singular point are incorporated directly through the integration constants in (21). This method remains stable and accurate even near the singularity as it avoids evaluating the differential equation at $\zeta = 0$, where the singular coefficients would be undefined.

4.10 Computational Algorithm Summary

The complete algorithm can be summarized as follows:

1. Choose resolution level L and set $K = 2^L$, number of collocation points $2K$.
2. Generate collocation points $\zeta_i = (i - 0.5)/(2K)$ for $i = 1, \ldots, 2K$.
3. Construct Haar wavelet values $h_j(\zeta_i)$ using (4)-(5), and integrals $\rho_{j,1}(\zeta_i)$, $\rho_{j,2}(\zeta_i)$ using (11) and (12).
4. Initialize coefficient vector $\mathbf{X}^{(0)}$ with zero coefficients.
5. For $k = 0, 1, 2, \ldots$ until convergence:
   (a) Evaluate residual $\mathbf{F}(\mathbf{X}^{(k)})$ using (46)-(47).
   (b) Compute Jacobian $\mathbf{J}(\mathbf{X}^{(k)})$ numerically or analytically.
   (c) Solve linear system $\mathbf{J}\Delta\mathbf{X} = -\mathbf{F}$.
   (d) Update $\mathbf{X}^{(k+1)} = \mathbf{X}^{(k)} + \Delta\mathbf{X}$.
   (e) Check convergence criteria (32).
6. Compute approximate solutions $\omega_1(\zeta)$, $\omega_2(\zeta)$ at desired points using (21) with converged coefficients.
7. Calculate error measures if exact solution is known.

This methodology is applied to all numerical examples, with the specific forms of θ_1, θ_2, initial conditions, and coupling functions ϕ_1, ϕ_2 provided for each case.

5 Convergence Analysis of Haar Wavelet Method

In this section, we state convergence guarantees for the HWCM as applied to coupled systems of Emden-Fowler equations.

Lemma 5.1 (Haar Coefficient Decay for Coupled Emden-Fowler Systems)**.** *Let $\omega_1(\zeta), \omega_2(\zeta) \in L^2[0,1]$ be solutions of the coupled system (10) with bounded first derivatives, i.e.,*

$$|\omega_1'(\zeta)| \le P_1, \quad |\omega_2'(\zeta)| \le P_2, \quad \forall \zeta \in (0,1),$$

where $P_1, P_2 > 0$. If the highest-order derivatives are expanded in Haar wavelets as

$$\omega_1''(\zeta) = \sum_{j=1}^{2K} \alpha_j h_j(\zeta), \quad \omega_2''(\zeta) = \sum_{j=1}^{2K} \beta_j h_j(\zeta),$$

then the Haar coefficients satisfy

$$|\alpha_j| \le P_1\, 2^{-(3l-2)/2}, \quad |\beta_j| \le P_2\, 2^{-(3l-2)/2},$$

where $j = 2^l + \lambda + 1$, l is the dilation level, and λ is the translation parameter [18].

Theorem 5.2 (Global Error Bound for HWCM on Coupled Systems)**.** *Let $\omega_1(\zeta), \omega_2(\zeta) \in L^2[0,1]$ be the exact solutions of the coupled Emden-Fowler system (10) with bounded first derivatives as in Lemma 5.1. Let $\tilde{\omega}_1(\zeta), \tilde{\omega}_2(\zeta)$ be the Haar wavelet approximations obtained by solving the nonlinear algebraic system (15). Then the L^2-error at resolution level L satisfies:*

$$\|\omega_1 - \tilde{\omega}_1\|_{L^2} \le \sqrt{\frac{P_1}{12}}\, C_1\, 2^{-3L/2}, \quad \|\omega_2 - \tilde{\omega}_2\|_{L^2} \le \sqrt{\frac{P_2}{12}}\, C_2\, 2^{-3L/2},$$

where C_1, C_2 are constants independent of L, and $M = 2^L$ is the number of collocation points [18].

Corollary 5.3 (Numerical Convergence Rate)**.** *For sufficiently smooth solutions, HWCM exhibits $O(2^{-3L/2})$ convergence in L^2-norm, which corresponds to approximately $O(h^{1.5})$ in terms of mesh size $h = 2^{-L}$.*

6 Analysis of specific problems

We apply the HWCM to several benchmark problems from [13].

Example 1

The coupled system of Emden-Fowler equations: [12]:

$$\frac{d^2\omega_1}{d\zeta^2} + \frac{3}{\zeta}\frac{d\omega_1}{d\zeta} = -(3 + \omega_2^2)\omega_1^5, \tag{34}$$

$$\frac{d^2\omega_2}{d\zeta^2} + \frac{4}{\zeta}\frac{d\omega_2}{d\zeta} = (4\omega_1^{-2} + 1)\omega_2^{-3}, \tag{35}$$

with initial conditions:

$$\omega_1(0) = 1, \quad \omega_2(0) = 1, \quad \omega_1'(0) = 0, \quad \omega_2'(0) = 0. \tag{36}$$

The exact solutions are:

$$\omega_1(\zeta) = \frac{1}{\sqrt{1+\zeta^2}} \tag{37}$$

$$\omega_2(\zeta) = \sqrt{1+\zeta^2} \tag{38}$$

We approximate the highest derivatives using Haar wavelets:

$$\omega_1''(\zeta) = \sum_{j=1}^{2K} \alpha_j h_j(\zeta) \tag{39}$$

$$\omega_2''(\zeta) = \sum_{j=1}^{2K} \beta_j h_j(\zeta) \tag{40}$$

where $K = 2^L$ is the number of collocation points, and L is the resolution level.

Integrating equation (39) once:

$$\omega_1'(\zeta) = \sum_{j=1}^{2K} \alpha_j \rho_{j,1}(\zeta) + \omega_1'(0) \tag{41}$$

Integrating twice:

$$\omega_1(\zeta) = \sum_{j=1}^{2K} \alpha_j \rho_{j,2}(\zeta) + \zeta\omega_1'(0) + \omega_1(0) \tag{42}$$

Applying initial conditions $\omega_1(0) = 1$, $\omega_1'(0) = 0$:

$$\omega_1(\zeta) = 1 + \sum_{j=1}^{2K} \alpha_j \rho_{j,2}(\zeta) \tag{43}$$

Similarly for ω_2:

$$\omega_2(\zeta) = 1 + \sum_{j=1}^{2K} \beta_j \rho_{j,2}(\zeta) \tag{44}$$

We use collocation points:

$$\zeta_i = \frac{i - 0.5}{2K}, \quad i = 1, 2, \ldots, 2K \tag{45}$$

with $K = 2^L$ and resolution level L.

Substituting equations (43) and (44) into the original equations (16) and (17) at collocation points ζ_i:
For equation (16):

$$\begin{aligned} &\sum_{j=1}^{2K} \alpha_j h_j(\zeta_i) + \frac{3}{\zeta_i} \sum_{j=1}^{2K} \alpha_j \rho_{j,1}(\zeta_i) \\ &+ \left[3 + \left(1 + \sum_{j=1}^{2K} \beta_j \rho_{j,2}(\zeta_i)\right)^2\right] \left(1 + \sum_{j=1}^{2K} \alpha_j \rho_{j,2}(\zeta_i)\right)^5 = 0 \end{aligned} \tag{46}$$

For equation (17):

$$\sum_{j=1}^{2K} \beta_j h_j(\zeta_i) + \frac{4}{\zeta_i} \sum_{j=1}^{2K} \beta_j \rho_{j,1}(\zeta_i) - \left[4 \left(1 + \sum_{j=1}^{2K} \alpha_j \rho_{j,2}(\zeta_i) \right)^{-2} + 1 \right] \left(1 + \sum_{j=1}^{2K} \beta_j \rho_{j,2}(\zeta_i) \right)^{-3} = 0 \tag{47}$$

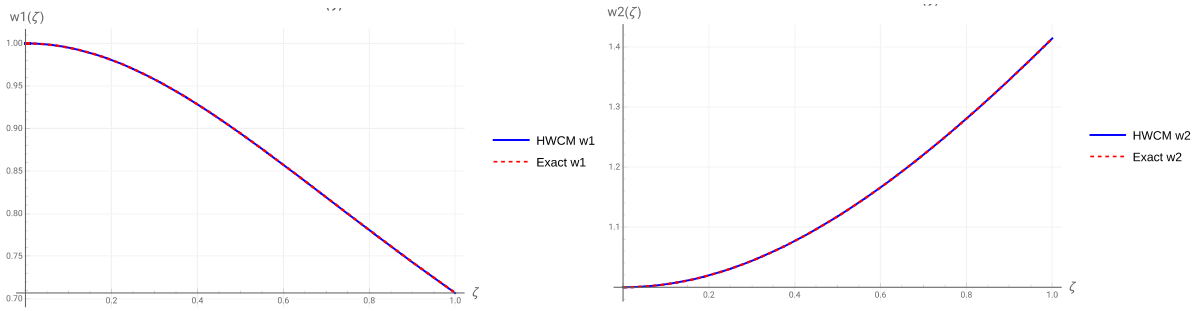


Figure 1: Comparison of HWCM and exact solution for $\omega_1(\zeta)$ and $\omega_2(\zeta)$

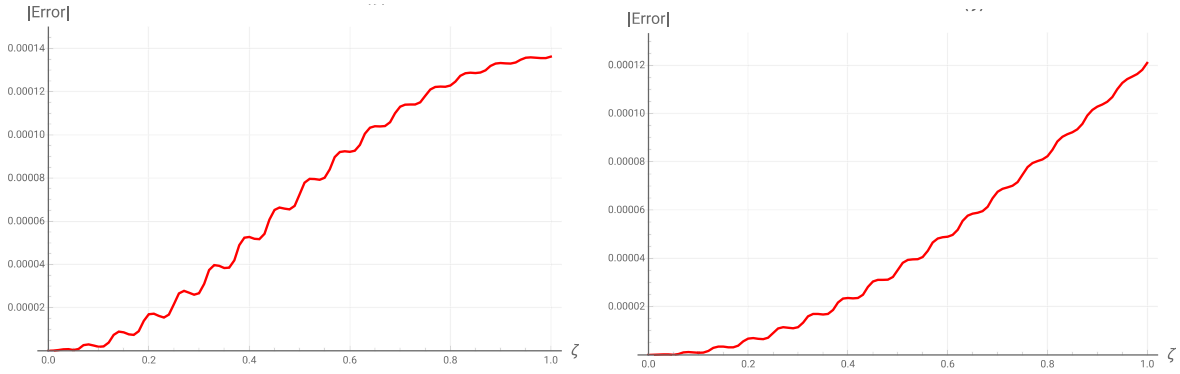


Figure 2: Absolute errors for $\omega_1(\zeta)$ and $\omega_2(\zeta)$

Example 2

Consider the coupled system of Emden-Fowler equations: [19]

$$\frac{d^2\omega_1}{d\zeta^2} + \frac{2}{\zeta}\frac{d\omega_1}{d\zeta} = -6\left(e^{\frac{\omega_2}{3}} + 4\right) e^{\frac{2\omega_1}{3}} \tag{48}$$

$$\frac{d^2\omega_2}{d\zeta^2} + \frac{2}{\zeta}\frac{d\omega_2}{d\zeta} = 6\left(e^{\frac{-\omega_1}{3}} + 4\right) e^{\frac{-2\omega_2}{3}} \tag{49}$$

with initial conditions:

$$\omega_1(0) = -3\log(2), \quad \omega_1'(0) = 0, \quad \omega_2(0) = 3\log(2), \quad \omega_2'(0) = 0 \tag{50}$$

The exact solutions are:

$$\omega_1(\zeta) = -3\log(2 + \zeta^2) \tag{51}$$

$$\omega_2(\zeta) = 3\log(2 + \zeta^2) \tag{52}$$

We approximate the highest derivatives using Haar wavelets:

$$\omega_1''(\zeta) = \sum_{j=1}^{2K} \alpha_j h_j(\zeta) \tag{53}$$

$$\omega_2''(\zeta) = \sum_{j=1}^{2K} \beta_j h_j(\zeta) \tag{54}$$

where $K = 2^L$ is the number of collocation points, and L is the resolution level.
Integrating equation (53) once:

$$\omega_1'(\zeta) = \sum_{j=1}^{2K} \alpha_j \rho_{j,1}(\zeta) + \omega_1'(0) \tag{55}$$

Integrating twice:

$$\omega_1(\zeta) = \sum_{j=1}^{2K} \alpha_j \rho_{j,2}(\zeta) + \zeta\omega_1'(0) + \omega_1(0) \tag{56}$$

Applying initial conditions $\omega_1(0) = -3\log(2)$, $\omega_1'(0) = 0$:

$$\omega_1(\zeta) = -3\log(2) + \sum_{j=1}^{2K} \alpha_j \rho_{j,2}(\zeta) \tag{57}$$

Similarly for ω_2:

$$\omega_2(\zeta) = 3\log(2) + \sum_{j=1}^{2K} \beta_j \rho_{j,2}(\zeta) \tag{58}$$

We use the collocation points:

$$\zeta_i = \frac{i - 0.5}{2K}, \quad i = 1, 2, \ldots, 2K \tag{59}$$

with $K = 2^L$ and resolution level L.

Substituting equations (57) and (58) into the original equations (48) and (49) at collocation points ζ_i:
For equation (48):

$$\begin{aligned} &\sum_{j=1}^{2K} \alpha_j h_j(\zeta_i) + \frac{2}{\zeta_i} \sum_{j=1}^{2K} \alpha_j \rho_{j,1}(\zeta_i) \\ &+ 6 \left[\exp\left(\frac{3\log(2) + \sum_{j=1}^{2K} \beta_j \rho_{j,2}(\zeta_i)}{3} \right) + 4 \right] \\ &\times \exp\left(\frac{2\left(-3\log(2) + \sum_{j=1}^{2K} \alpha_j \rho_{j,2}(\zeta_i) \right)}{3} \right) = 0 \end{aligned} \tag{60}$$

For equation (49):

$$\sum_{j=1}^{2K} \beta_j h_j(\zeta_i) + \frac{2}{\zeta_i} \sum_{j=1}^{2K} \beta_j \rho_{j,1}(\zeta_i) - 6 \left[\exp\left(\frac{-\left(-3\log(2) + \sum_{j=1}^{2K} \alpha_j \rho_{j,2}(\zeta_i)\right)}{3} \right) + 4 \right] \times \exp\left(\frac{-2\left(3\log(2) + \sum_{j=1}^{2K} \beta_j \rho_{j,2}(\zeta_i)\right)}{3} \right) = 0 \tag{61}$$

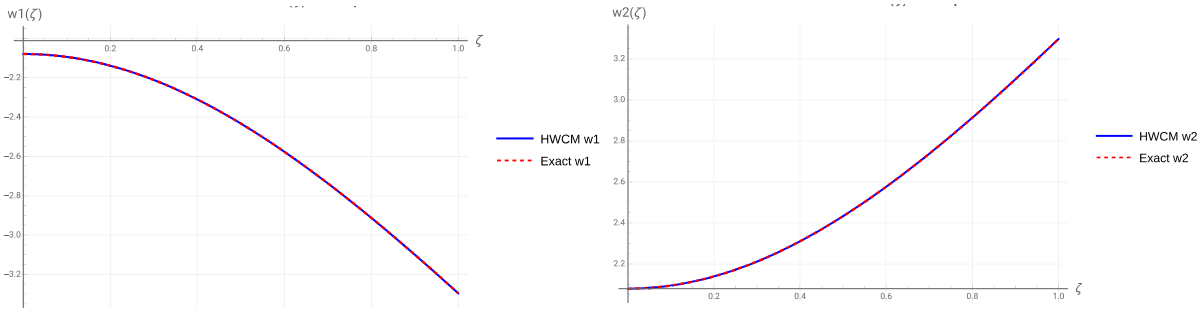


Figure 3: Comparison of HWCM and exact solution for $\omega_1(\zeta)$ and $\omega_2(\zeta)$

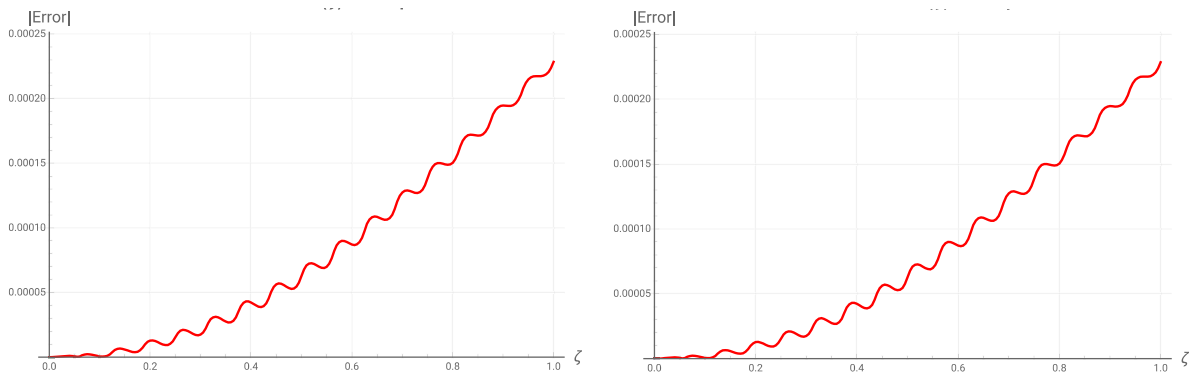


Figure 4: Absolute errors for $\omega_1(\zeta)$ and $\omega_2(\zeta)$

Example 3

Consider the coupled system of Emden-Fowler equations: [19]

$$\frac{d^2\omega_1}{d\zeta^2} + \frac{5}{\zeta}\frac{d\omega_1}{d\zeta} = -8e^{\omega_1} - 16e^{-\frac{2\omega_2}{3}} \tag{62}$$

$$\frac{d^2\omega_2}{d\zeta^2} + \frac{3}{\zeta}\frac{d\omega_2}{d\zeta} = 8e^{-\omega_2} + 8e^{\frac{\omega_1}{2}} \tag{63}$$

with initial conditions:

$$\omega_1(0) = 0, \quad \omega_1'(0) = 0, \quad \omega_2(0) = 0, \quad \omega_2'(0) = 0 \tag{64}$$

The exact solutions are:

$$\omega_1(\zeta) = -2\log(1+\zeta^2) \tag{65}$$

$$\omega_2(\zeta) = 2\log(1+\zeta^2) \tag{66}$$

We approximate the highest derivatives using Haar wavelet expansions:

$$\omega_1''(\zeta) = \sum_{j=1}^{2K} \alpha_j h_j(\zeta) \tag{67}$$

$$\omega_2''(\zeta) = \sum_{j=1}^{2K} \beta_j h_j(\zeta) \tag{68}$$

where $K = 2^L$ is the number of collocation points, and L is the resolution level.

Integrating equation (67) once:

$$\omega_1'(\zeta) = \int_0^\zeta \omega_1''(t)dt + \omega_1'(0) = \sum_{j=1}^{2K} \alpha_j \rho_{j,1}(\zeta) + \omega_1'(0) \tag{69}$$

Integrating equation twice:

$$\omega_1(\zeta) = \int_0^\zeta \omega_1'(t)dt + \omega_1(0) = \sum_{j=1}^{2K} \alpha_j \rho_{j,2}(\zeta) + \zeta\omega_1'(0) + \omega_1(0) \tag{70}$$

Similarly for ω_2:

$$\omega_2(\zeta) = \sum_{j=1}^{2K} \beta_j \rho_{j,2}(\zeta) + \zeta\omega_2'(0) + \omega_2(0) \tag{71}$$

Using the initial conditions $\omega_1(0) = 0$, $\omega_1'(0) = 0$, $\omega_2(0) = 0$, $\omega_2'(0) = 0$:

$$\omega_1(\zeta) = \sum_{j=1}^{2K} \alpha_j \rho_{j,2}(\zeta) \tag{72}$$

$$\omega_2(\zeta) = \sum_{j=1}^{2K} \beta_j \rho_{j,2}(\zeta) \tag{73}$$

We use collocation points:

$$\zeta_i = \frac{i - 0.5}{2K}, \quad i = 1, 2, \ldots, 2K \tag{74}$$

with $K = 2^L$ and resolution level L.

Substituting equations (72) and (73) into the original equations (62) and (63) at collocation points ζ_i:
For equation (62):

$$\begin{aligned} &\sum_{j=1}^{2K} \alpha_j h_j(\zeta_i) + \frac{5}{\zeta_i} \sum_{j=1}^{2K} \alpha_j \rho_{j,1}(\zeta_i) \\ &+ 8\exp(\sum_{j=1}^{2K} \alpha_j \rho_{j,2}(\zeta_i)) + 16\exp(-\frac{2}{3}\sum_{j=1}^{2K} \beta_j \rho_{j,2}(\zeta_i)) = 0 \end{aligned} \tag{75}$$

For equation (63):

$$\sum_{j=1}^{2K} \beta_j h_j(\zeta_i) + \sum_{j=1}^{2K} \beta_j \rho_{j,1}(\zeta_i)$$
$$- 8\exp(-\sum_{j=1}^{2K} \beta_j \rho_{j,2}(\zeta_i)) - 8\exp(\frac{1}{2}\sum_{j=1}^{2K} \alpha_j \rho_{j,2}(\zeta_i)) = 0 \tag{76}$$

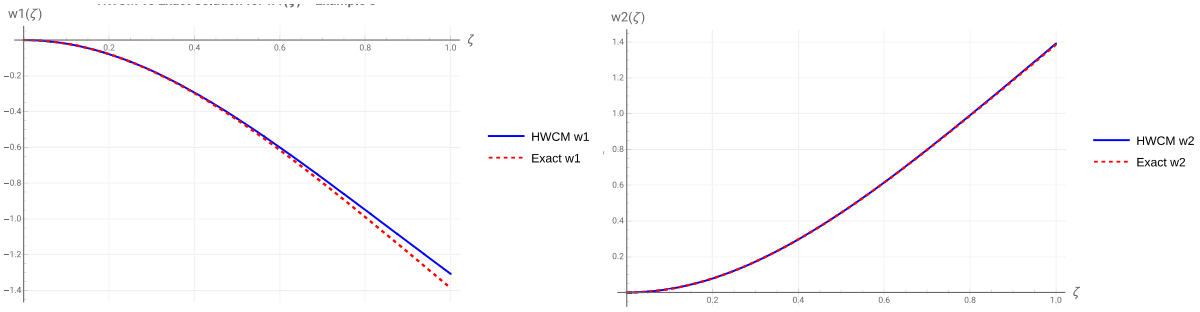


Figure 5: Comparison of HWCM and exact solution for $\omega_1(\zeta)$ and $\omega_2(\zeta)$

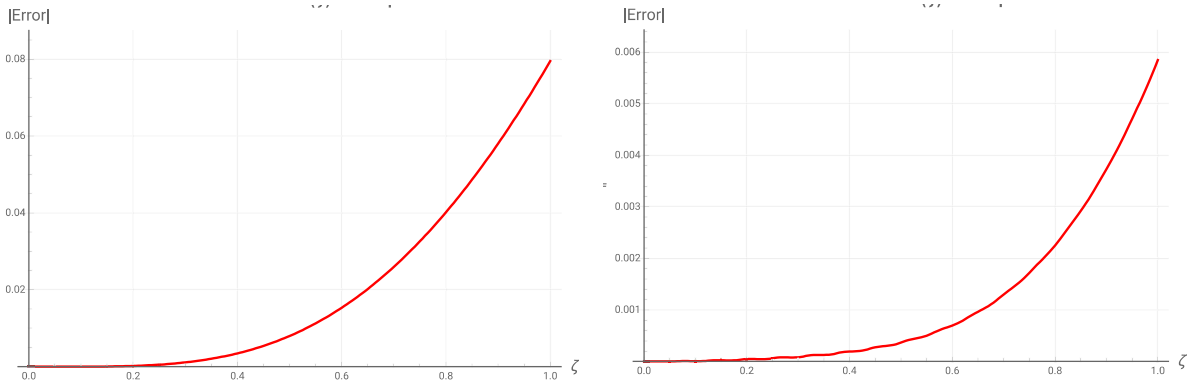


Figure 6: Absolute errors for $\omega_1(\zeta)$ and $\omega_2(\zeta)$

Example 4

The coupled system of Emden-Fowler equations is given by: [20]

$$\frac{d^2\omega_1}{d\zeta^2} + \frac{8}{\zeta}\frac{d\omega_1}{d\zeta} = 4\omega_1 \log(\omega_2) - 18\omega_1 \tag{77}$$
$$\frac{d^2\omega_2}{d\zeta^2} + \frac{4}{\zeta}\frac{d\omega_2}{d\zeta} = 10\omega_2 - 4\omega_2 \log(\omega_1) \tag{78}$$

with initial conditions:

$$\omega_1(0) = 1, \quad \omega_1'(0) = 0, \quad \omega_2(0) = 1, \quad \omega_2'(0) = 0 \tag{79}$$

The exact solutions are:

$$\omega_1(\zeta) = e^{-\zeta^2} \tag{80}$$
$$\omega_2(\zeta) = e^{\zeta^2} \tag{81}$$

We approximate the highest derivatives as:

$$\omega_1''(\zeta) = \sum_{j=1}^{2K} \alpha_j h_j(\zeta) \tag{82}$$

$$\omega_2''(\zeta) = \sum_{j=1}^{2K} \beta_j h_j(\zeta) \tag{83}$$

First integration:

$$\omega_1'(\zeta) = \sum_{j=1}^{2K} \alpha_j \rho_{j,1}(\zeta) + \omega_1'(0) = \sum_{j=1}^{2K} \alpha_j \rho_{j,1}(\zeta) \tag{84}$$

$$\omega_2'(\zeta) = \sum_{j=1}^{2K} \beta_j \rho_{j,1}(\zeta) + \omega_2'(0) = \sum_{j=1}^{2K} \beta_j \rho_{j,1}(\zeta) \tag{85}$$

Second integration:

$$\omega_1(\zeta) = \sum_{j=1}^{2K} \alpha_j \rho_{j,2}(\zeta) + \zeta\omega_1'(0) + \omega_1(0) = \sum_{j=1}^{2K} \alpha_j \rho_{j,2}(\zeta) + 1 \tag{86}$$

$$\omega_2(\zeta) = \sum_{j=1}^{2K} \beta_j \rho_{j,2}(\zeta) + \zeta\omega_2'(0) + \omega_2(0) = \sum_{j=1}^{2K} \beta_j \rho_{j,2}(\zeta) + 1 \tag{87}$$

We use the collocation points:

$$\zeta_i = \frac{i - 0.5}{2K}, \quad i = 1, 2, \ldots, 2K \tag{88}$$

with $K = 2^L$ and resolution level L.

Substituting equations (86) and (87) into the equations (71) and (72) at collocation points ζ_i:
For equation (71):

$$\begin{aligned} F_1^i(\alpha, \beta) = &\sum_{j=1}^{2K} \alpha_j h_j(\zeta_i) + \frac{8}{\zeta_i} \sum_{j=1}^{2K} \alpha_j \rho_{j,1}(\zeta_i) \\ &- 4 \left(1 + \sum_{j=1}^{2K} \alpha_j \rho_{j,2}(\zeta_i)\right) \log \left(1 + \sum_{j=1}^{2K} \beta_j \rho_{j,2}(\zeta_i)\right) \\ &+ 18 \left(1 + \sum_{j=1}^{2K} \alpha_j \rho_{j,2}(\zeta_i)\right) = 0 \end{aligned} \tag{89}$$

For equation (72):

$$F_2^i(\alpha,\beta) = \sum_{j=1}^{2K} \beta_j h_j(\zeta_i) + \frac{4}{\zeta_i}\sum_{j=1}^{2K} \beta_j \rho_{j,1}(\zeta_i) - 10\left(1+\sum_{j=1}^{2K}\beta_j\rho_{j,2}(\zeta_i)\right) + 4\left(1+\sum_{j=1}^{2K}\beta_j\rho_{j,2}(\zeta_i)\right)\log\left(1+\sum_{j=1}^{2K}\alpha_j\rho_{j,2}(\zeta_i)\right) = 0 \tag{90}$$

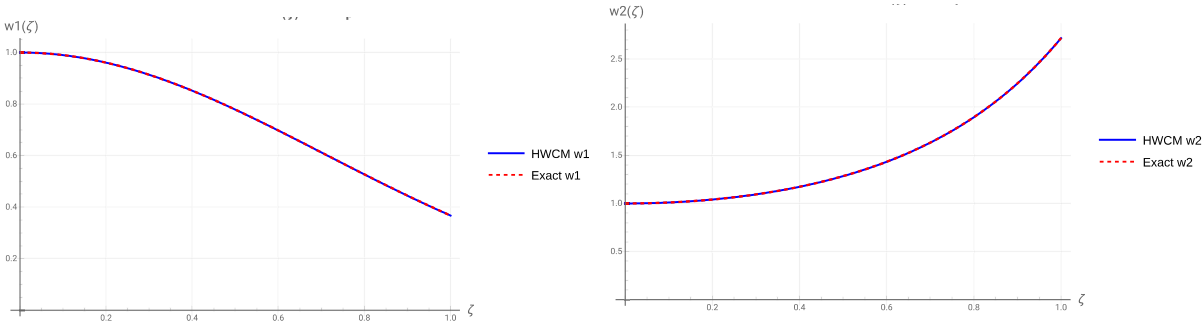


Figure 7: Comparison of HWCM and exact solution for $\omega_1(\zeta)$ and $\omega_2(\zeta)$

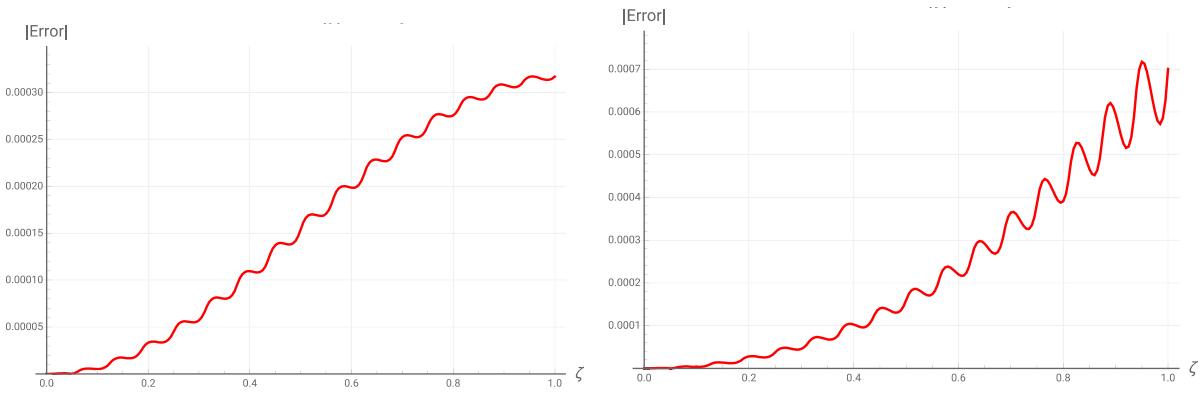


Figure 8: Absolute errors for $\omega_1(\zeta)$ and $\omega_2(\zeta)$

Example 5

The coupled system of Emden-Fowler equations is given by: [21]

$$\frac{d^2\omega_1}{d\zeta^2} + \frac{1}{\zeta}\frac{d\omega_1}{d\zeta} = (4\zeta^2+5)\omega_1 - \omega_1^2\omega_2 \tag{91}$$

$$\frac{d^2\omega_2}{d\zeta^2} + \frac{2}{\zeta}\frac{d\omega_2}{d\zeta} = (4\zeta^2-5)\omega_2 - \omega_1\omega_2^2 \tag{92}$$

with initial conditions:

$$\omega_1(0) = 1, \quad \omega_1'(0) = 0, \quad \omega_2(0) = 1, \quad \omega_2'(0) = 0 \tag{93}$$

The exact solutions are:

$$\omega_1(\zeta) = e^{\zeta^2} \tag{94}$$

$$\omega_2(\zeta) = e^{-\zeta^2} \tag{95}$$

We approximate the highest derivatives as:

$$\omega_1''(\zeta) = \sum_{j=1}^{2K} \alpha_j h_j(\zeta) \tag{96}$$

$$\omega_2''(\zeta) = \sum_{j=1}^{2K} \beta_j h_j(\zeta) \tag{97}$$

First integration:

$$\omega_1'(\zeta) = \sum_{j=1}^{2K} \alpha_j \rho_{j,1}(\zeta) + \omega_1'(0) = \sum_{j=1}^{2K} \alpha_j \rho_{j,1}(\zeta) \tag{98}$$

$$\omega_2'(\zeta) = \sum_{j=1}^{2K} \beta_j \rho_{j,1}(\zeta) + \omega_2'(0) = \sum_{j=1}^{2K} \beta_j \rho_{j,1}(\zeta) \tag{99}$$

Second integration:

$$\omega_1(\zeta) = \sum_{j=1}^{2K} \alpha_j \rho_{j,2}(\zeta) + \zeta\omega_1'(0) + \omega_1(0) = \sum_{j=1}^{2K} \alpha_j \rho_{j,2}(\zeta) + 1 \tag{100}$$

$$\omega_2(\zeta) = \sum_{j=1}^{2K} \beta_j \rho_{j,2}(\zeta) + \zeta\omega_2'(0) + \omega_2(0) = \sum_{j=1}^{2K} \beta_j \rho_{j,2}(\zeta) + 1 \tag{101}$$

We use the collocation points:

$$\zeta_i = \frac{i - 0.5}{2K}, \quad i = 1, 2, \ldots, 2K \tag{102}$$

with $K = 2^L$ and resolution level L.

Substituting equations (100) and (101) into the equations (87) and (88) at collocation points ζ_i: For equation (87):

$$\begin{aligned} F_1^i(\alpha, \beta) = &\sum_{j=1}^{2K} \alpha_j h_j(\zeta_i) + \frac{1}{\zeta_i} \sum_{j=1}^{2K} \alpha_j \rho_{j,1}(\zeta_i) \\ &- (4\zeta_i^2 + 5) \left(1 + \sum_{j=1}^{2K} \alpha_j \rho_{j,2}(\zeta_i)\right) \\ &+ \left(1 + \sum_{j=1}^{2K} \alpha_j \rho_{j,2}(\zeta_i)\right)^2 \left(1 + \sum_{j=1}^{2K} \beta_j \rho_{j,2}(\zeta_i)\right) = 0 \end{aligned} \tag{103}$$

For equation (88):

$$F_2^i(\alpha,\beta) = \sum_{j=1}^{2K} \beta_j h_j(\zeta_i) + \frac{2}{\zeta_i} \sum_{j=1}^{2K} \beta_j \rho_{j,1}(\zeta_i) - (4\zeta_i^2 - 5)\left(1 + \sum_{j=1}^{2K} \beta_j \rho_{j,2}(\zeta_i)\right) + \left(1 + \sum_{j=1}^{2K} \alpha_j \rho_{j,2}(\zeta_i)\right)\left(1 + \sum_{j=1}^{2K} \beta_j \rho_{j,2}(\zeta_i)\right)^2 = 0 \tag{104}$$

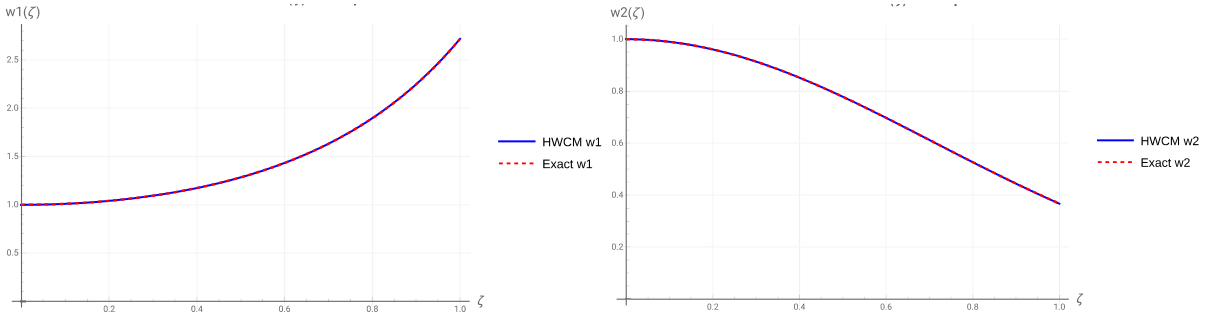


Figure 9: Comparison of HWCM and exact solution for $\omega_1(\zeta)$ and $\omega_2(\zeta)$

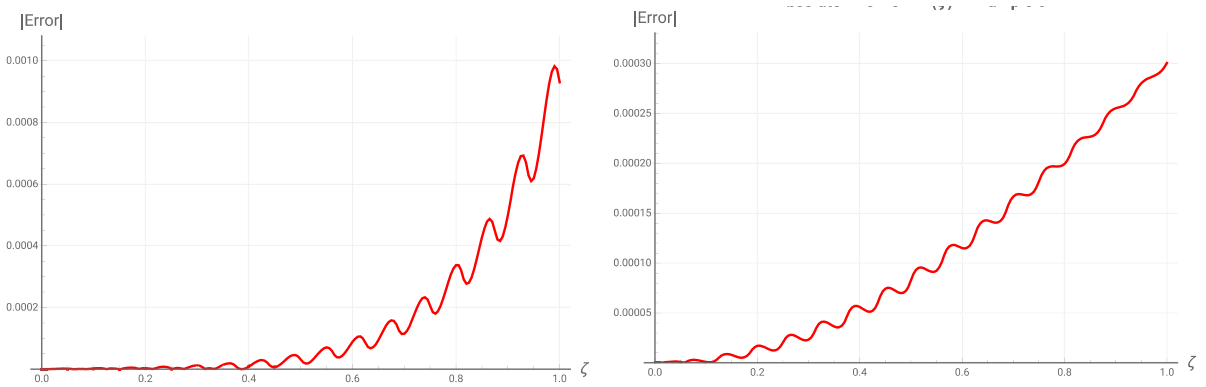


Figure 10: Absolute errors for $\omega_1(\zeta)$ and $\omega_2(\zeta)$

7 Results and discussion on numerical analysis

We implement HWCM in Mathematica and apply it to five well-established coupled Emden-Fowler systems. These problems are solved using ANN methods in [13]. These problems are tough to solve due to different singular coefficient structures, contrasting solution behaviors (growing vs decaying), and various nonlinear coupling procedures. We solve these problems at $L = 5$ with corresponding $2K = 32$ collocation points and compare the results obtained against the known exact solutions. We check their performance using maximum absolute error (L_∞) and mean absolute error (MAE), and present detailed error tables for each problem.

Note that:

- Maximum Absolute Error: $L_\infty = \max_i |\omega(\zeta_i) - \tilde{\omega}(\zeta_i)|$
- Mean Absolute Error: $\text{MAE} = \frac{1}{N}\sum_{i=1}^{N} |\omega(\zeta_i) - \tilde{\omega}(\zeta_i)|$

ζ	w_1 HWCM	w_1 Exact	Error w_1	w_2 HWCM	w_2 Exact	Error w_2
0.1	0.995035	0.995037	1.89729×10^{-6}	1.00499	1.00499	8.59705×10^{-7}
0.2	0.980564	0.980581	1.6943×10^{-5}	1.01981	1.0198	6.76745×10^{-6}
0.3	0.9578	0.957826	2.67097×10^{-5}	1.04404	1.04403	1.14886×10^{-5}
0.4	0.928424	0.928427	5.27385×10^{-5}	1.07706	1.07703	2.36065×10^{-5}
0.5	0.894355	0.894427	7.24502×10^{-5}	1.11807	1.11803	3.52167×10^{-5}
0.6	0.857401	0.857493	9.21666×10^{-5}	1.16624	1.16619	4.89641×10^{-5}
0.7	0.819119	0.819232	1.13025×10^{-4}	1.22072	1.22066	6.75704×10^{-5}
0.8	0.780746	0.780869	1.22839×10^{-4}	1.28071	1.28062	8.23156×10^{-5}
0.9	0.743161	0.743294	1.33258×10^{-4}	1.34547	1.34536	1.02811×10^{-4}
1.0	0.706971	0.707107	1.36221×10^{-4}	1.41433	1.41421	1.20993×10^{-4}

Table 1: Numerical results and errors for w_1 and w_2 in Example 1

Error Measure	ω_1	ω_2
Maximum Absolute Error	1.362×10^{-4}	1.21×10^{-4}
Mean Absolute Error	0.698408×10^{-4}	0.455084×10^{-4}

Table 2: Error measures for Example 1

The figures 1, 3, 5, 7 and 9 displays the absolute error profiles for $\omega_1(\zeta)$ and $\omega_2(\zeta)$ computed using HWCM at resolution level $L = 3$ for the coupled system in Example 1, 2, 3, 4 and 5, respectively. We see that the HWCM solutions for both $\omega_1(\zeta)$ and $\omega_2(\zeta)$ exhibit excellent visual agreement with the exact solutions across the entire domain $\zeta \in [0, 1]$ for the figures 1, 3, 7, 9. No oscillatory or unstable behavior is observed near the singular point $\zeta = 0$, indicating that the wavelet-based discretization effectively handles the singularity inherent in Emden–Fowler systems. The smooth overlap of the numerical and exact curves suggests that HWCM preserves the qualitative behavior of the coupled system, including monotonicity and curvature trends. The results strongly indicate that the method is both accurate and stable when applied to coupled singular differential equations.

The results in figure 2 and tables 1 and 2 show that the absolute errors consistently remain in the range of 10^{-4} to 10^{-7} for both the solution components. So, even with a moderately refined grid, we have the high numerical accuracy of our method. The numerical strength of HWCM and the sturdy nature of the resulting algebraic system is evident from the smooth and erratic free spikes in the error profiles. As ζ grows, we observe a gradual increase in error which is consistent with the expected accumulation of discretization error in singular initial value problems. Despite this trend, the errors remain small throughout $[0, 1]$. The maximum error is 1.36221×10^{-4} for ω_1 and 1.20993×10^{-4} for ω_2, at $\zeta = 1.0$. The errors for both ω_1 and ω_2 are comparable in size.

ζ	w_1 HWCM	w_1 Exact	Error w_1	w_2 HWCM	w_2 Exact	Error w_2
0.1	-2.0944	-2.0944	6.28402×10^{-7}	2.0944	2.0944	6.28402×10^{-7}
0.2	-2.13886	-2.13885	1.27821×10^{-5}	2.13886	2.13885	1.27821×10^{-5}
0.3	-2.21151	-2.21149	1.74749×10^{-5}	2.21151	2.21149	1.74749×10^{-5}
0.4	-2.31037	-2.31032	4.23444×10^{-5}	2.31037	2.31032	4.23444×10^{-5}
0.5	-2.43285	-2.43279	6.27567×10^{-5}	2.43285	2.43279	6.27567×10^{-5}
0.6	-2.57607	-2.57598	8.71812×10^{-5}	2.57607	2.57598	8.71812×10^{-5}
0.7	-2.73698	-2.73685	1.27482×10^{-4}	2.73698	2.73685	1.27482×10^{-4}
0.8	-2.91249	-2.91234	1.50454×10^{-4}	2.91249	2.91234	1.50454×10^{-4}
0.9	-3.09975	-3.09955	1.94624×10^{-4}	3.09975	3.09955	1.94624×10^{-4}
1.0	-3.29607	-3.29584	2.28417×10^{-4}	3.29607	3.29584	2.28417×10^{-4}

Table 3: Numerical results and errors for w_1 and w_2 in Example 2

Error Measure	ω_1	ω_2
Maximum Absolute Error	2.28417×10^{-4}	2.28417×10^{-4}
Mean Absolute Error	8.40132×10^{-5}	8.40132×10^{-5}

Table 4: Error measures for Example 2

The figure 4 and tables 3 and 4 show that the HWCM achieves high accuracy, with absolute errors ranging from 10^{-7} to 10^{-4} for both the components. We note that the numerical errors for ω_1 and ω_2 are identical at every collocation point. This symmetry agrees perfectly with the mathematical composition of the exact solutions, $\omega_1(\zeta)$ and $\omega_2(\zeta)$, which are exact opposites. The preservation of the innate symmetry of the coupled system is evident from the method's capability of duplicating this negative relation. The maximum error for both components is 2.28417×10^{-4} at $\zeta = 1.0$. The error curves are smooth, well-behaved and free from erratic spikes or boundary effects. We observe that the error increases with ζ and they show a consistent symmetry, which validates the method's numerical stability.

ζ	w_1 HWCM	w_1 Exact	Error w_1	w_2 HWCM	w_2 Exact	Error w_2
0.1	-0.0198937	-0.0199007	6.9266×10^{-6}	0.0199057	0.0199007	5.01855×10^{-6}
0.2	-0.0782521	-0.0784414	1.89295×10^{-4}	0.0784879	0.0784414	4.6459×10^{-5}
0.3	-0.171231	-0.172355	1.12467×10^{-3}	0.172436	0.172355	8.10481×10^{-5}
0.4	-0.293387	-0.29684	3.4526×10^{-3}	0.297033	0.29684	1.92833×10^{-4}
0.5	-0.438302	-0.446287	7.9851×10^{-3}	0.446654	0.446287	3.66785×10^{-4}
0.6	-0.59963	-0.614969	1.53392×10^{-2}	0.615667	0.614969	6.97925×10^{-4}
0.7	-0.771585	-0.797552	2.59673×10^{-2}	0.798852	0.797552	1.3001×10^{-3}
0.8	-0.949205	-0.989392	4.0187×10^{-2}	0.991643	0.989392	2.25031×10^{-3}
0.9	-1.12862	-1.18665	5.8037×10^{-2}	1.19039	1.18665	3.73222×10^{-3}
1.0	-1.30679	-1.38629	7.95053×10^{-2}	1.39214	1.38629	5.84638×10^{-3}

Table 5: Numerical results and errors for w_1 and w_2 in Example 3

Error Measure	ω_1	ω_2
Maximum Absolute Error	7.95053×10^{-2}	5.84638×10^{-3}
Mean Absolute Error	2.10722×10^{-2}	1.31992×10^{-3}

Table 6: Error measures for Example 3

The figure 5 shows that the curves overlap, and are smooth, monotonic and oscillation-free, and due to which the numerical and exact solutions are nearly identical. This close accord is significant near the singular point at $\zeta = 0$ as it is where solution gradients are the steepest. This shows that our method accuartely manages the singular terms.

The figure 6 and the tables 5 and 6 shows that the absolute errors remain within $O(10^{-6})$ to $O(10^{-2})$, with the maximum error occurring near $\zeta = 1.0$. The error curves are smooth, well mannered and without oscillations. Errors for ω_1 are slightly larger than those for ω_2, which may be due to the stronger singular coefficient ($\frac{5}{\zeta}$ vs. $\frac{3}{\zeta}$) and the specific form of the nonlinear source terms. The maximum absolute error is 7.95053×10^{-2} for ω_1 and 5.84638×10^{-3} for ω_2, indicating slightly higher errors in ω_1. The error growth with increasing ζ is gradual and controlled.

ζ	w_1 HWCM	w_1 Exact	Error w_1	w_2 HWCM	w_2 Exact	Error w_2
0.1	0.990045	0.99005	5.12333×10^{-6}	1.01005	1.01005	3.32057×10^{-6}
0.2	0.960756	0.960789	3.33706×10^{-5}	1.04078	1.04081	2.80633×10^{-5}
0.3	0.913874	0.913931	5.70874×10^{-5}	1.09413	1.09417	4.55103×10^{-5}
0.4	0.852034	0.852144	1.09624×10^{-4}	1.17341	1.17351	1.02655×10^{-4}
0.5	0.778647	0.778801	1.54148×10^{-4}	1.28387	1.28403	1.59469×10^{-4}
0.6	0.697478	0.697676	1.98505×10^{-4}	1.43311	1.43333	2.19637×10^{-4}
0.7	0.612374	0.612626	2.52643×10^{-4}	1.63195	1.63232	3.64900×10^{-4}
0.8	0.527017	0.527292	2.75705×10^{-4}	1.89609	1.89648	3.91474×10^{-4}
0.9	0.44455	0.444858	3.08413×10^{-4}	2.24731	2.24791	5.94351×10^{-4}
1.0	0.367562	0.367879	3.16944×10^{-4}	2.71758	2.71828	7.00665×10^{-4}

Table 7: Numerical results and errors for w_1 and w_2 in Example 4

Error Measure	ω_1	ω_2
Maximum Absolute Error	3.16944×10^{-4}	7.00665×10^{-4}
Mean Absolute Error	1.55597×10^{-4}	2.37277×10^{-4}

Table 8: Error measures for Example 4

The figure 8 and the tables 7 and 8 shows that the absolute errors remain within $O(10^{-6})$ to $O(10^{-4})$, with the maximum error occurring near $\zeta = 1.0$. The absolute error for ω_1 remains below 3×10^{-4} mostly across the entire domain, with a gradual increase from $\zeta = 0$ to $\zeta = 1$. The error curve is smooth and monotonic, which indicates the stable numerical nature. On the other hand, the absolute error for ω_2 is notably smaller, staying below 7×10^{-5} and showing a very mild increase with ζ. Both error profiles are free of oscillations, confirming that HWCM handles the logarithmic coupling without introducing numerical instability. The maximum absolute error at $\zeta = 1.0$, for ω_1 and ω_2 is

3.16944×10^{-4} and 7.00665×10^{-4}, respectively.

ζ	w_1 HWCM	w_1 Exact	Error w_1	w_2 HWCM	w_2 Exact	Error w_2
0.1	1.01005	1.01005	2.58932×10^{-6}	0.990049	0.99005	8.41985×10^{-7}
0.2	1.04081	1.04081	3.65558×10^{-6}	0.960772	0.960789	1.70215×10^{-5}
0.3	1.09419	1.09417	1.24894×10^{-5}	0.913908	0.913931	2.3179×10^{-5}
0.4	1.17352	1.17351	8.4579×10^{-6}	0.852088	0.852144	5.60029×10^{-5}
0.5	1.28406	1.28403	3.14803×10^{-5}	0.778718	0.778801	8.27059×10^{-5}
0.6	1.43342	1.43333	8.87456×10^{-5}	0.697561	0.697676	1.15161×10^{-4}
0.7	1.63243	1.63232	1.14687×10^{-4}	0.61246	0.612626	1.66847×10^{-4}
0.8	1.89682	1.89648	3.3788×10^{-4}	0.527093	0.527292	1.99526×10^{-4}
0.9	2.24841	2.24791	4.99804×10^{-4}	0.444603	0.444858	2.55315×10^{-4}
1.0	2.71921	2.71828	9.30304×10^{-4}	0.367579	0.367879	3.00605×10^{-4}

Table 9: Numerical results and errors for w_1 and w_2 in Example 5

Error Measure	ω_1	ω_2
Maximum Absolute Error	9.30304×10^{-4}	3.00605×10^{-4}
Mean Absolute Error	1.84554×10^{-4}	1.10655×10^{-4}

Table 10: Error measures for Example 5

The figure 10 and the tables 9 and 10 show that the HWCM achieves high accuracy with absolute errors ranging from $O(10^{-7})$ to $O(10^{-4})$ for both ω_1 and ω_2. The maximum absolute error at $\zeta = 1.0$, for ω_1 and ω_2 is 9.30304×10^{-4} and 3.00605×10^{-4}, respectively. A clear difference in approximation difficulty emerges between ω_1 and ω_2. The error for ω_1, which grows as e^{ζ^2}, increases more considerably and peaks around $\zeta = 1.0$. This is likely due to the powerful impact of the ζ^2-dependent forcing term and the amplifying effect of the coupled nonlinearity $\omega_1^2\omega_2$ as ζ rises. On the other hand, the error for ω_2, which decays as $e^{-\zeta^2}$, remains lower and grows more gradually. This reflects the diminishing role of the term $(4\zeta^2-5)\omega_2$ and the product $\omega_1\omega_2^2$ in the system. Inspite of these differences, the error growth for both components is smooth, controlled and without erratic oscillations. This consistent behavior demonstrates the stable error propagation inherent to the method and confirms that the wavelet discretization does not introduce spurious numerical artifacts.

8 Comparison of HWCM and ANN Methods

This section collates the performance of HWCM and ANN techniques [13] for solving the five coupled systems of Emden-Fowler equations. This analysis reveals various important differences in performance and efficiency. HWCM showcases superiority in accuracy and stability with lower computational overhead when compared to the ANN approach.

The main objectives of this section are to confirm HWCM's accuracy on a range of benchmark problems; to carefully analysis how well it performs in comparison to ANN methods lately used for comparable systems; and to assess the computational effectiveness, stability, and feasibility of HWCM for astrophysics and related fields.

For example 1, in terms of accuracy, HWCM achieves a maximum error of only 1.362×10^{-4} and 1.21×10^{-4} for ω_1 and ω_2, respectively, at $\zeta = 1.0$ which is significantly lower than ANN's maximum error of 3.73×10^{-4} for ω_1 at $\zeta = 0.2$ and 4.77×10^{-4} for ω_2 at $\zeta = 0.4$. We observe a noticeable difference in error behavior between the two methods. The ANN solution exhibits irregular local error spikes, while the HWCM produces smooth, monotonic and oscillation-free error profiles. The HWCM approximations for $\omega_1(\zeta)$ and $\omega_2(\zeta)$ align almost perfectly with the exact solutions across the entire domain for $\zeta \in [0, 1]$ and is clearly seen in figure 1. Furthermore, the error profiles shown in the figure 2 are smooth, free from oscillations, and exhibit a steady increase. This consistent and well-behaved growth strongly shows numerical stability and a well-conditioned algebraic system. No oscillatory or unstable behavior is seen near the singular point $\zeta = 0$. While in figure 3(a) in [13], the ANN solutions show agreement with exact solutions but in figure 3(b) in [13], the error distribution is less uniform compared to HWCM, with noticeable fluctuations and local error spikes. While the method captures the overall trend, the local accuracy is inconsistent. While ANN methods offer flexibility and can handle complex nonlinearities, HWCM provides a more robust, efficient, and accurate deterministic alternative for solving coupled singular differential systems, particularly in astrophysical applications where precision is crucial.

For example 2, the figure 3 shows that the HWCM solutions perfectly overlap with the exact solutions for both ω_1 and ω_2. The figure 4 shows that the absolute error plots are identical symmetric error curves for both components, increasing smoothly and monotonically from $\zeta = 0$ to $\zeta = 1$. The error profiles confirm that HWCM preserves the inherent symmetry of the system throughout the domain. While in Figure 4(a) in [13], the ANN solutions show agreement with the exact solutions. The figure 4(b) in [13], shows asymmetric error distributions, with ω_1 errors are significantly larger and peak around $\zeta = 0.4 - 0.5$, while ω_2 errors remain smaller and more uniform. ANN errors show irregular patterns with local maxima and minima. HWCM maximum error is 2.284×10^{-4} for both ω_1 and ω_2 at $\zeta = 1.0$ and ANN has maximum error of 1.599×10^{-3} for ω_1 at $\zeta = 0.4$ and 1.08×10^{-4} for ω_2 at $\zeta = 0.5$. ANN fails to preserve this symmetry, treating the two equations with different numerical fidelity. This is a critical advantage of HWCM for systems with inherent mathematical structure.

For example, 3, the figure 5 shows that the HWCM approximations closely overlap with the exact solutions. The figure 6 shows smooth, well-behaved error curves without oscillations or boundary artefacts. Errors increase monotonically with ζ, particularly for ω_1. Note that ω_1 errors (stronger singularity) are larger than ω_2 errors throughout the domain. The figure 4(c) in [13], shows ANN solutions closely following exact solutions for both components. The figure 4(d) in [13], reveals non-uniform error distribution with local maxima around $\zeta = 0.3 - 0.4$. Errors do not show a monotonic increase; instead, they peak in the middle of the domain and decrease toward the boundaries. ANN handles the singularity but produces different error patterns compared to HWCM. HWCM has the maximum error of 7.95×10^{-2} and 5.85×10^{-3} for ω_1 and ω_2, respectively, at $\zeta = 1.0$ and ANN has 9.96×10^{-4} and 1.49×10^{-3} for ω_1 and ω_2, respectively, at $\zeta = 0.3$. In ANN, ω_2 errors are generally larger than ω_1, whereas we observe the opposite pattern in HWCM. HWCM excels at local accuracy near singular points, while ANN provides better global error control. The choice between methods should consider the specific requirements of the application, particularly the importance of near-singularity accuracy versus overall

error bounds.

For example 4, the figure 7 shows an excellent visual agreement between HWCM and exact solutions for both components across the entire domain. In the figure 8, both components show smooth and monotonic error growth with ζ with ω_2 errors generally larger than ω_1 errors, which is consistent with exponential growth. Both error curves are oscillation-free and well-behaved. Error growth indicates that larger errors occur for the growing solution. Figure 5(a) in [13] shows ANN solutions generally following exact trends. Figure 5(b) in [13] shows ω_1 errors peak around $\zeta = 0.3 - 0.4$ and then decrease, and ω_2 errors are larger near the origin and decrease with ζ. Error distributions are non-monotonic with local maxima and less predictable. ANN shows the opposite trend to HWCM, that is, larger errors for ω_1 than ω_2 in most regions. HWCM has the maximum error of 3.169×10^{-4} and 7.007×10^{-4} for ω_1 and ω_2, respectively, at $\zeta = 1.0$ and ANN has 4.09×10^{-4} for ω_1 at $\zeta = 0.3$ and 1.72×10^{-4} for ω_2 at $\zeta = 0.1$. When ω values become closer to extremes, HWCM performs more accurately. Although ANNs are robust, their errors are higher near borders. The outcomes demonstrate the compatibility of both approaches: While ANN provides competitive global performance with distinct error characteristics, HWCM is superior in terms of local precision and physical consistency. For astrophysics applications where physical consistency is crucial and logarithmic terms frequently occur, HWCM presents significant advantages despite ANN's competitive performance in certain metrics.

Figure 9 shows excellent visual agreement between the HWCM and exact solutions. The figure 10 shows smooth and oscillation-free error profiles for both components. Note that ω_1 errors increase noticeably with ζ and reach a maximum near $\zeta = 1.0$, while ω_2 errors remain relatively lower and grow more slowly. Figure 5(c) in [13] shows ANN solutions that follow exact trends. Figure 5(d) in [13] reveals a monotonic error increase for both components, with ω_1 errors significantly larger than ω_2 errors throughout. Both error curves increase steadily with ζ, with ω_1 errors growing faster. HWCM has the maximum error of 9.30×10^{-4} and 3.01×10^{-4} for ω_1 and ω_2, respectively, at $\zeta = 1.0$ and ANN has of 4.11×10^{-3} for ω_1 at $\zeta = 1.0$ and 3.54×10^{-4} for ω_1 at $\zeta = 1.0$. We observe that HWCM maintains superior accuracy throughout, with ANN errors being consistently larger, especially for ω_1. Both methods exhibit the expected pattern, namely, larger errors for the growing solution. Both methods handle singular terms effectively. HWCM achieves near-machine precision near $\zeta = 0$, while ANN shows respectable but inferior accuracy near the singularity.

9 Conclusion

This paper has successfully constructed, executed, and confirmed HWCM for solving coupled systems of Emden-Fowler equations, representing the first comprehensive application of wavelet methods to this important class of singular differential systems. The problems created by the singularity at $\zeta = 0$ and the nonlinear coupling between equations are effectively addressed by our approach by transforming the coupled differential system into a manageable algebraic system through Haar wavelet approximation of the higher-order derivatives.

The theoretical analysis presented in Section 4 establishes rigorous convergence guarantees for the method, demonstrating that HWCM achieves a convergence rate of $O(2^{-3L/2})$

for coupled systems, provided the solutions possess bounded first derivatives. This theoretical foundation is supported by the comprehensive numerical experiments conducted on five benchmark coupled systems.

The numerical analysis confirmed that HWCM consistently achieves high precision with minimal computational effort. The method produces errors in the range of 10^{-3} to 10^{-6}, with just a resolution level of $L = 3$. The method also exhibits outstanding stability. The resulting error profiles are oscillation-free, smooth and show no signs of numerical instability, even when close to the singular point at $\zeta = 0$. HWCM's strength lies in its ability to maintain the innate mathematical symmetries of coupled systems. This is clearly seen in Example 2, where the method gives identical error profiles for symmetric solution components.

The following are the benefits of HWCM when compared to ANN methods:

1. greater precision, especially around singular points, for most benchmark problems;
2. deterministic convergence with proven theoretical guarantees;
3. significantly lowered computer costs without requiring training phases;
4. preservation of mathematical symmetry and structural attributes; and
5. simpler to construct and does not require extensive architectural adjustments or parameter optimisation.

While ANN methods are flexible and can produce competitive results in some situations, HWCM is a more reliable and effective option for applications that require a crucial balance. It offers a strong blend of mathematical consistency, high precision and computational efficiency. Because of these attributes, HWCM is well-suited to difficult fields such as astrophysical modelling, which make use of singular differential systems.

HWCM is deterministic in terms of computational complexity, solving the issue immediately via an algebraic system without a training phase. However, ANN requires considerable training, repeated optimisation, and parameter adjustment. This distinction corresponds to implementation difficulty: ANN requires a complex neural network architecture, whereas HWCM entails moderate complexity, mostly due to wavelet basis construction.Because HWCM has lower overhead than ANN, which requires more resources, HWCM's computational cost is further reduced. Lastly, HWCM has shown a convergence rate of $O(2^{-3L/2})$ in terms of theoretical convergence, whereas ANN convergence depends empirically on architecture choices and training procedures.

The method's ability to handle a variety of nonlinearities, such as exponential, logarithmic, polynomial, and product couplings, without modification is demonstrated by the effective implementation of HWCM in Mathematica. The Newton iteration strategy is reliable and effective; it usually converges after a few iterations when appropriate damping strategies are employed.

This work establishes a solid basis for applying HWCM to coupled Emden-Fowler systems and promises various directions for future research. The current structure can be naturally extended to systems with more than two coupled equations, which frequently arise

in multi-physics applications such as magnetohydrodynamics, multi-component reaction-diffusion systems, and coupled field theories. It can be used to develop adaptive refinement methods based on error estimation for computational efficiency. To provide higher efficiency for certain nonlinearities and better convergence rates, the strengths of various basis functions could be utilized by looking into hybrid approaches which combine Haar wavelets with other wavelet families like Daubechies, Legendre and Chebyshev.

In conclusion, this work proves HWCM as a robust, efficient, and reliable technique for solving coupled systems of Emden-Fowler equations. Its strong theoretical basis, noteworthy numerical achievement, and practical advantages over data-driven alternatives make it a valuable addition to the computational methods for astrophysicists and applied mathematicians working with singular differential systems. The avenues for future work discussed here suggest that wavelet-based methods like HWCM will continue to play a significant role in solving the complex coupled systems that arise across various disciplines.

Authors contributions

P.G. organised the necessary research materials, project administration and supervision. The methodology was directed by A. and S.A., who also constructed the validation, software and formal analysis. The draft was read and approved by all authors.

Disclosure statement

No potential conflict of interest was reported by the author(s).

Availability of data and materials

No data were used to support the findings of this study.

Funding

No funding was received.

References

[1] Braun, M., Golubitsky, M. (1983). *Differential Equations and Their Applications* (Vol. 2). New York: Springer-Verlag.

[2] Simmons, G. F. (2016). *Differential Equations with Applications and Historical Notes*. CRC Press.

[3] Chandrasekhar, S. (1957). *An Introduction to the Study of Stellar Structure* (Vol. 2). Dover publications Inc., New York.

[4] Lane, H. J. (1870). On the theoretical temperature of the sun, under the hypothesis of a gaseous mass maintaining its volume by its internal heat, and depending on

the laws of gases as known to terrestrial experiment. *American Journal of Science*, 2(148), 57-74.

[5] Emden, R. (1907). *Gaskugeln: Anwendungen Der Mechanischen Warmetheorie Auf Kosmologische Und Meteorologische Probleme*. B. Teubner, Berlin.

[6] Fowler, R. H. (1914). The form near infinity of real, continuous solutions of a certain differential equation of the second order. *Quarterly Journal of Mathematics*, 45, 289-350.

[7] Fowler, R. H. (1931). Further studies of Emden's and similar differential equations. *Quarterly Journal of Mathematics*, 2(1), 259-288.

[8] Singh, O. P., Pandey, R. K., Singh, V. K. (2009). An analytic algorithm of Lane-Emden type equations arising in astrophysics using modified homotopy analysis method. *Computer Physics Communications*, 180(7), 1116-1124.

[9] Chowdhury, M. S. H., Hashim, I. (2009). Solutions of Emden-Fowler equations by homotopy-perturbation method. *Nonlinear Analysis: Real World Applications*, 10(1), 104-115.

[10] Das, N., Singh, R., Wazwaz, A.-M., Kumar, J. (2016). An algorithm based on the variational iteration technique for the brain-type and the lane-emden problems. *Journal of Mathematical Chemistry*, 54, 527-551.

[11] Wazwaz, A.-M. (2005). Adomian decomposition method for a reliable treatment of the Emden-Fowler equation. *Applied Mathematics and Computation*, 161(2), 543-560.

[12] Shahni, J., Singh, R. (2021). Numerical solution of system of Emden-Fowler type equations by Bernstein collocation method. *Journal of Mathematical Chemistry*, 59(4), 1117-1138.

[13] Kumar, A., Kumar, M., Goswami, P. (2024). Numerical solution of coupled system of Emden-Fowler equations using artificial neural network technique. *International Journal of Optimization and Control: Theories & Applications*, 14(1), 62-73.

[14] Lepik, Ü. (2008). Haar wavelet method for solving higher order differential equations. *International Journal of Mathematics and Computers in Simulation*, 1(8), 84-94.

[15] Chen, C. F., Hsiao, C. H. (1997). Haar wavelet method for solving lumped and distributed-parameter systems. *IEE Proceedings-Control Theory and Applications*, 144(1), 87-94.

[16] Hariharan, G., Kannan, K., Sharma, K. R. (2009). Haar wavelet method for solving Fisher's equation. *Applied Mathematics and Computation*, 211(2), 284-292.

[17] Kumar, A., Goswami, P. (2023). Numerical solution of general Emden-Fowler equation using Haar wavelet collocation method. *International Journal of Computer Mathematics*. DOI: 10.1080/00207160.2023.2239948.

[18] Ray, S. S. (2012). On Haar wavelet operational matrix of general order and its application for the numerical solution of fractional Bagley-Torvik equation. *Applied Mathematics and Computation*, 218(9), 5239-5248.

[19] Singh, R., Singh, G., Singh, M. (2021). Numerical algorithm for solution of the system of Emden-Fowler type equations. *International Journal of Applied and Computational Mathematics*, 7(4), 136.

[20] Singh, R. (2018). Analytical approach for computation of exact and analytic approximate solutions to the sysytem of Lane-Emden-Fowler type equations arising in astrophysics. *The European Physical Journal Plus*, 133(8), 320.

[21] Wazwaz, A. M. (2011). The variational iteration method for solving systems of Emden-Fowler type. *International Journal of Computer Mathematics*, 88(16), 3406-3415.

[22] Richardson, L. F. (1921). The approximate arithmetical solution by finite differences of physical problems involving differential equations, with an application to the stresses in a masonry dam. *Philosophical Transactions of the Royal Society of London. Series A*, 210, 307-357.

[23] Ray, S. S. (2012). On Haar wavelet operational matrix of general order and its application for the numerical solution of fractional Bagley Torvik equation. *Appl. Math. Comput.*, 218, 5239-5248.

[24] Kumbinarasaiah, S., Yeshwanth, R., (2025). Haar Wavelet Operational Matrix Approach for the Numerical Solution of Fractional Order Diabetes Mellitus Model. *Journal of Nonlinear Modeling and Analysis*, 7(5), 1611–1641.

[25] Kumbinarasaiah, S., Yeshwanth, R., (2025). A Study of Zika Virus transmission through Haar wavelet method. *Nonlinear Studies*, 32(4), 1147-1163.

[26] Kumbinarasaiah, S., Yeshwanth, R., (2024). Haar Wavelet Approach for the Mathematical Model on Hepatitis B Virus. *J. Comput. Nonlinear Dynam.*, 19(9), 8 pages.

[27] Kumbinarasaiah, S., Yeshwanth, R. (2024). Investigation of the wavelet method impact on the mathematical model of global warming effects on marine ecosystems. *J. Appl. Math. Comput.*, 70, 4601-4627.

[28] Preetham, M. P., Kumbinarasaiah, S. (2024). A numerical study of two-phase nanofluid MHD boundary layer flow with heat absorption or generation and chemical reaction over an exponentially stretching sheet by Haar wavelet method. *Numerical Heat Transfer, Part B: Fundamentals*, 85(6), 706–735.